RESEARCH ARTICLE

FASEB BioAdvances WILEY

Antioxidants restore store-operated Ca^{2+} entry in patient-iPSC-derived myotubes with tubular aggregate myopathy-associated Ile484ArgfsX21 STIM1 mutation via upregulation of binding immunoglobulin protein

Fusako Sakai-Takemura[1] | Fumiaki Saito[2] | Ken'ichiro Nogami[1,3] |
Yusuke Maruyama[1,4] | Ahmed Elhussieny[1,5] | Kiichiro Matsumura[2] |
Shin'ichi Takeda[1] | Yoshitsugu Aoki[1] | Yuko Miyagoe-Suzuki[1]

[1]Department of Molecular Therapy, National Institute of Neuroscience, National Center of Neurology and Psychiatry, Tokyo, Japan

[2]Department of Neurology, School of Medicine, Teikyo University, Tokyo, Japan

[3]Department of Neurology, Neurological Institute, Graduate School of Medical Science, Kyushu University, Fukuoka, Japan

[4]Department of Gene Regulation, Faculty of Pharmaceutical Science, Tokyo University of Science, Chiba, Japan

[5]Department of Neurology, Faculty of Medicine, Minia University, Minia, Egypt

Correspondence
Yuko Miyagoe-Suzuki, Department of Molecular Therapy, National Institute of Neuroscience, National Center of Neurology and Psychiatry, Tokyo, Japan.
Email: miyagoe@ncnp.go.jp

Abstract

Store-operated Ca^{2+} entry (SOCE) is indispensable for intracellular Ca^{2+} homeostasis in skeletal muscle, and constitutive activation of SOCE causes tubular aggregate myopathy (TAM). To understand the pathogenesis of TAM, we induced pluripotent stem cells (iPSCs) from a TAM patient with a rare mutation (c.1450_1451insGA; p. Ile484ArgfsX21) in the *STIM1* gene. This frameshift mutation produces a truncated STIM1 with a disrupted C-terminal inhibitory domain (CTID) and was reported to diminish SOCE. Myotubes induced from the patient's-iPSCs (TAM myotubes) showed severely impaired SOCE, but antioxidants greatly restored SOCE partly via upregulation of an endoplasmic reticulum (ER) chaperone, BiP (GRP78), in the TAM myotubes. Our observation suggests that antioxidants are promising tools for treatment of TAM caused by reduced SOCE.

KEYWORDS
antioxidants, binding immunoglobulin protein, calcium, calcium release-activated calcium channel protein 1 (ORAI1), induced pluripotent stem cells, skeletal muscle, store-operated Ca^{2+} entry, Stromal interaction molecule 1, tubular aggregate myopathy

---

1 | INTRODUCTION

Store-operated Ca^{2+} entry (SOCE) is a fundamental mechanism required for Ca^{2+} homeostasis in skeletal muscle. Depletion of Ca^{2+} stores in the endoplasmic and sarcoplasmic reticulum (ER/SR) is sensed by a single-pass transmembrane ER protein, STIM1, via its luminal Ca^{2+}-binding EF-hands (cEF and hEF) and sterile alpha motif (SAM) domain.[1,2] Ca^{2+} depletion induces conformation changes of STIM1 and promotes its oligomerization. The conformation changes also expose the channel activation domain (CAD), which interacts with a Ca^{2+}-release-activated Ca^{2+} (CRAC) channel, ORAI1, located in transverse tubules to trigger extracellular Ca^{2+} entry.[3,4] Elevated cytosolic Ca^{2+} is then taken up into the ER/SR by the sarco/endoplasmic reticulum Ca^{2+}-ATPase (SERCA) pump. To prevent Ca^{2+} overload, fast (~10–20 ms) and slow (~1–3 min) Ca^{2+}-dependent inactivations (FCDI and SCDI, respectively) are triggered upon elevation of cytoplasmic Ca^{2+}. SCDI is facilitated by SOCE-associated regulatory factor (SARAF) binding to the STIM1-Orai1 activating region (SOAR) of STIM1, and its binding is controlled by acidic residues in the C-terminal inhibitory domain (CTID).[5] The CTID also inactivates STIM1 in resting conditions by interacting with the coiled-coil domain1 (CC1).[6]

Gain-of-function mutations in the *STIM1* and *ORAI1* genes cause tubular aggregate myopathy (TAM; OMIM#160565 and 615883) with constitutively active SOCE.[7–12] In contrast, recessive loss-of-function mutations in the STIM1 gene result in insufficient SOCE and cause severe immunodeficiency.[13] TAM is characterized by progressive muscle weakness with reduced resistance to fatigue, muscle atrophy, myalgia, and pathologically by the appearance of tubular aggregates, which appear red on Gomori trichrome staining and exhibit a honeycomb structure of densely packed tubules on electron microscopy in skeletal muscle. To date, almost all TAM-related STIM1 mutations are missense mutations in the Ca^{2+}-binding EF-hand (cEF and hEF) motif of the luminal region and the cytoplasmic coiled-coil domain 1 (CC1).[14] Mutations in EF-hands disrupt Ca^{2+} binding and therefore constitutively activate Ca^{2+} entry through ORAI1. The $STIM1^{R304W}$ mutation in the CC1 domain destabilizes the tight conformation of STIM1, promotes the exposure of the SOAR domain, enhances the CC1-CC1 homodimerization, and activates ORAI1 even when there is enough Ca^{2+} stock in the ER/SR.[14]

In 2016, Okuma et al.[15] reported a novel autosomal dominant mutation in the cytoplasmic domain of STIM1, creating a truncated STIM1 protein (c.1450_1451insGA; p. Ile484ArgfsX21) with a disrupted CTID. The patient showed no Stomorken syndrome signs, such as miosis, thrombocytopenia, hyposplenism, ichthyosis, short stature, or dyslexia, and no history of repetitive infections indicative of immunodeficiency. Although the phenotype was similar to TAM caused by common gain-of-function mutations of *STIM1*, the mutant *STIM1* gene reduced SOCE when overexpressed in C2C12 cells or HEK293 cells. Recently, Kim et al.[16] reported that the same mutation enhanced SOCE when co-expressed with wild-type ORAI1 in human primary myoblasts or HEK293T cells. Here, we established induced pluripotent stem cells (iPS cells) from the patient, because skeletal muscle derived from the patient-iPSCs is expected to express both the wild-type and the mutant STIM1 together with wild-type ORAI1 at physiologic levels. Myotubes induced from the patient-iPSCs showed a weak SOCE response. We also found that BiP expression is reduced in TAM myotubes, and that antioxidants can restore SOCE partly via upregulation of BiP. Our results suggest that antioxidants could be therapeutic tools for TAM patients with reduced SOCE.

2 | MATERIALS AND METHODS

2.1 | Control human iPS cells

409B2, 454E2, and 201B7 iPSC lines established from healthy donors were provided by Prof. Shinya Yamanaka at the Center for iPS Cell Research and Application (CiRA), Kyoto University.[17–19] 201B7-PAX7-Venus was provided by Dr. Hidetoshi Sakurai at CiRA.[20]

2.2 | Establishment of TAM-iPSCs

TAM-specific iPSCs were established following the CiRA protocol (https://www.cira.kyoto-u.acjp/j/research/img/protocol/Episomal_Blood_Protocol.pdf). In brief, peripheral blood mononuclear cells (PBMCs) from the TAM patient[15] were cultured in StemSpan H300 (Stem Cell Technologies) with 100 μg/mL of IL-6 (Pepro Tech), 300 μg/mL each of SFC (Pepro Tech), TPO (Pepro Tech), Flt3 ligand (Pepro Tech), and 10 μg/mL of IL-3 (Pepro Tech). After a 6-day culture, a cocktail of episomal plasmids (pCE-hOCT3/4, pCE-hSK, pCE-hUL, pCE-mp53DD, and pCXB-EBNA1) was transfected to PBMCs by using a Nucleofector II Device (Lonza). Four weeks later, colonies were picked up and cultured in StemFit AK02N medium (Ajinomoto) on iMatrix-511 (Nippi Inc.)-coated 6-well plates. Induced iPSC-like cells were immunostained with OCT3/4, SOX2, and NANOG

antibodies (Cell Signaling). Mycoplasma infection was routinely tested using a PCR Mycoplasma Detection Set (Takara). For plasmid vector integration checks, genomic DNAs were extracted by a DNeasy Blood & Tissue Kit (QIAGEN) and amplified by PCR primers (pEP4-SF1: 5′-TTCCACGAGGGTAGTGAACC-3′, pEP4-SR1: 5′-TCGGGGGTGTTAGAGACAAC-3′) using Ex-Taq (Takara).[21] G-band karyotyping was performed by Nihon Gene Research Laboratories Inc. (http://ngrl.co.jp/). The gene mutation was confirmed by Sanger sequencing at Eurofins Genomics (http://eurofinsgenomics.jp). More information on antibodies is shown in Table S1. For teratoma formation tests, $1-2 \times 10^6$ iPS cells were subcutaneously injected into the backs of anesthetized Nod-Scid mice. Formed teratomas were dissected, fixed with 4% paraformaldehyde (PFA), and sectioned. Frozen sections 8 μm-thick were incubated with α-fetoprotein (Santa Cruz), βIII-tubulin (Abcam), α-smooth muscle actin (Dako), or with anti-human specific Lamin A/C antibody (Leica). The paraffin embedded sections were stained with hematoxylin and eosin. TAM-iPS cells passaged fewer than 10 times were used for analysis.

2.3 | Derivation of skeletal muscle progenitors from human iPS cells

Muscle induction from human iPSCs was performed as previously described[22] with modification. hiPSCs were plated on iMatrix-511-coated 6-well plates at a density of 240,000 cells/well and cultured in Di-CL medium (DMEM/F12 supplemented with 1% v/v Insulin-Transferrin-Selenium; ITS, Gibco), 3 μM CHIR-99021 (Tocris), and 0.5 μM LDN-193189 (Stemgent) for 3 d and then in Di-CLF medium (Di-CL medium supplemented with 20 ng/mL FGF-2; Pepro Tech) for 3 d.[23,24] Then, cells were detached using a cell scraper (Iwaki) and transferred to ultra-low attachment surface flasks (Corning) in Stemline medium (S-3194; Sigma-Aldrich) supplemented with 100 ng/mL bFGF (Pepro Tech), 100 ng/mL EGF (Pepro Tech), 5 μg/mL heparin sodium salt (Sigma-Aldrich), and 1% v/v penicillin/streptomycin/amphotericin B (PSA; Wako).[25] After 6 weeks floating culture, the medium was changed to Stemline supplemented with 1 μM SB431542 and 1% v/v PSA and cultured for 4 weeks. After 4-week culture in growth factor-free medium, spheres were again cultured for 2 weeks in the growth factor-rich medium. During floating culture, spheres were weekly chopped into 200 μm cubes by a McIlwain tissue chopper (Mickle Laboratory Engineering).

2.4 | FACS analysis and cell sorting

FACS analysis and sorting were performed as described.[22,26] In brief, after a 1-week adhesion culture of spheres in the differentiation medium (10% fetal bovine serum and 1 μM SB431542 in Dulbecco's modified Eagle's medium; DMEM), cells detached from dishes using 0.05% trypsin were incubated with the following antibodies: CD82-APC (Miltenyi Biotec), ERBB3-APC (BD Pharmingen), CD271-BB515 (BD Pharmingen), or isotype control antibodies (1:200 dilution each) for 30 min at 4°C. After washing with 0.2%FBS/PBS (−) buffer, cells were analyzed and sorted by using BD FACSAria Fusion. Data were analyzed by FACS Diva (BD Bioscience, v8.0) and FlowJo software (BD Biosciences). CD271$^+$CD82$^+$ cells were collected by FACS as myogenic cells. For myotube formation, cells were plated onto collagen-coated dishes (Iwaki) in 10% FBS/DMEM/PSA/1 μM SB431542. More information on antibodies is shown in Table S1.

2.5 | Immunocytochemistry

Cells were fixed by 4% PFA (Nacalai Tesque) for 15 min at room temperature (RT) and permeated with 0.1% TritonX-100 (Sigma-Aldrich) for 10 min. After blocking with 5% goat serum (Cedarlane)/2% bovine serum albumin (Sigma-Aldrich) in PBS for 15 min at 37°C, cells were incubated with primary antibodies overnight at 4°C. The next day, the cells were washed with PBS and incubated with secondary antibodies for 2 h at RT. Nuclei were stained with DAPI (Tokyo Chemical Industry) at 1:10,000 dilution. Images were taken using a KEYENCE BZ-X810 microscope and analyzed by cell count software (Keyence) and ImageJ Fiji (NIH). The antibodies used are listed in Table S1.

2.6 | RT-qPCR

RT-qPCR was performed as previously described.[22,26] In brief, total RNA was extracted from cells with a RNeasy Mini Kit (Qiagen) and reverse transcribed into cDNA using PrimeScript RT reagent kit (Takara). cDNA was amplified with SYBR Premix EX Taq II (Til RNaseH Plus, Takara) and the primers listed in Table S2. The signal was recorded with a CFX Connect Real-Time System (Bio-Rad) and analyzed using the comparative C_t method ($2^{-\Delta\Delta C_t}$). Raw C_t values of target genes were normalized to C_t values of glyceraldehyde-3-phosphate dehydrogenase (GAPDH). Then, the Delta–Delta C_t value was calculated

by normalizing the C_t value of each gene to that of the human skeletal muscle total RNA (Clontech, Cat#636534; lot 1502315A).

2.7 | Time-lapse Ca^{2+} imaging

Ca^{2+} in ER/SR was labeled by lentiviral transduction of pLV-CAG-R-CEPIA1er-IRES-Puro (Sirion Biotech). For cytosolic Ca^{2+} imaging, myotubes cultured for 10 days in differentiation medium were loaded with 4 µM Fura-2/AM (Dojindo Laboratories) in imaging solution (107 mM NaCl, 6 mM KCl, 1.2 mM MgCl$_2$, 2 mM CaCl$_2$, 11.5 mM glucose, and 20 mM HEPES pH 7.4) for 40 min at 37°C. Images were captured using an inverted microscope (IX83; Olympus) with a perfusion system at 10-s intervals. Fura-2 (excitation filters D340X and D380X/ emitter D510/40) and rCEPIA1er (TRITC/Cy3 filter) fluorescence images were recorded with MetaMorph Imaging Software (Molecular Devices). The images were analyzed by ImageJ Fiji software (NIH). SOCE was induced by a Ca^{2+}-free imaging solution containing 0.5 mM EGTA or 5 µM thapsigargin (Nacalai Tesque). Ca^{2+} release from the ER/SR via RyR was stimulated by 50 mM caffeine in the imaging solution.

2.8 | Immunoblotting

Cells were lysed in a lysis buffer containing 316 mM NaCl, 20 mM Tris–HCl (pH 7.2), 2 mM EGTA, 0.2% SDS, 2% sodium deoxycholate, and 2% Triton X-100 with cOmplete Mini protease inhibitor cocktail (Roche) and PhosSTOP EASYpack (Roche). After centrifugation at 10,000 g, 4°C for 5 min, the supernatant protein was quantified by the Bradford method (Bio-Rad Protein Assay Dye Reagent, Cat#500-0006). Sample buffer (×6) (0.35 M Tis-HCl (pH 6.8), 10% SDS, 30% glycerol, and 9.3% DTT) was added to the cell lysate and heated at 100°C for 5 min. Proteins were resolved on a 10% Tris-glycine gel (Bio-Rad Protean TGX gel, Cat#4561033) and transferred to polyvinylidene difluoride (PVDF) membranes (Merck Millipore). The membranes were then blocked in TBS-0.1% Tween20 (TBST) containing 3% non-fat dry milk (Wako, Cat#190-12865) for 1 h at RT and incubated with primary antibodies overnight at 4°C. After washing in TBST, the membranes were incubated with secondary antibodies diluted 1:2000, for 30 min at RT. After washing, the membranes were reacted with the ECL Prime Western Blotting Detection Reagent (GE Healthcare) or SuperSignal West Dura Extended Duration Substrate (Thermo Scientific). The signals were detected by a ChemiDoc MP Imaging System (BioRad). For analysis of ER stress, an ER stress antibody sampler kit (Cell Signaling) was used according to the manufacturer's instructions.

2.9 | Quantification of protein carbonyls

Protein carbonyl levels in myotubes were evaluated with an OxyBlot protein oxidation detection kit (Millipore) according to the manufacturer's protocol. In brief, carbonyl groups in the protein side chains were derivatized by 2,4-dinitrophenylhydrazine (DNPH). Immunoblotting was then performed with an antibody against DNP. α-Tubulin (T6199; Sigma-Aldrich) was used as a loading control.

2.10 | Immunoprecipitation

Cells were lysed in a NP40 lysis buffer, containing 10 mM Tris–HCl (pH 7.4), 150 mM NaCl, 0.5 mM EDTA, and 1% Nonidet P40 (Nacalai Tesque) with cOmplete Mini protease inhibitor cocktail (Roche) and PhosSTOP EASY pack (Roche). The lysates were incubated with an anti-STIM1 antibody (sc-166840; Santa Cruz) overnight at 4°C on a rocking platform. After 16 h, lysates were incubated with protein G-Sepharose beads (Amersham Biosciences) for 1 h at 4°C. The beads were then collected by centrifugation at 12,000 g for 5 min. The proteins were dissolved by NP40 lysis buffer containing with 2% β-mercaptoethanol for OxyBlot.

2.11 | Measurement of intracellular reactive oxygen species (ROS) level

The intracellular ROS level was measured using the fluorescent oxidant-sensitive probe 2′7-dichlorofluorescenin diacetate (DCFDA; Invitrogen). After myotube formation, 20 µM DCFDA was added to the culture and incubated for 30 min at 37°C. The ROS signals (green fluorescence) were detected with a Keyence BZ X-810 fluorescence microscope. As a positive control, 0.5 mM H$_2$O$_2$ was added to the culture and incubated for 30 min at 37°C.

2.12 | MTT assay

MTT (3-[4,5-dimethylthiazol-2-yl]-2,5 diphenyl tetrazolium bromide) was assayed as described in a previous report.[27] In brief, cells were plated at a density of 2×10^4 cells/well in 96-well collagen-coated plates. After

myotube formation, 0.05 mg/mL MTT was added to the culture, and it was incubated for 3 h in a CO_2 incubator. After aspiration of the medium, acid isopropanol was added to each well, and the well contents were transferred to 1.5 mL tubes and centrifuged. OD_{590} of the supernatant was measured by a Synergy HTX Multi-Mode Reader (BioTek). Untreated wells were used as a control.

2.13 | Proximity ligation assay (PLA)

In situ PLA was performed with Duolink In Situ PLA Probes (Sigma-Aldrich) according to the manufacturer's protocol. SOCE was induced using 5 μM thapsigargin, and cells were and immediately fixed with 4% PFA in PBS (Nacalai Tesque) for 15 min at RT. Then, the cells were washed with PBS and permeabilized by 0.5% Triton X-100 in PBS for 10 min. Following washing with 0.05% Tween 20 in TBS, the cells were blocked with the blocking buffer for 1 h at 37°C. Then, cells were incubated with mouse anti-STIM1 antibody (sc-166840; Santa Cruz) and rabbit anti-ORAI1 antibody (O8262, Sigma-Aldrich) diluted 1:100 in Duolink Antibody Diluent solution overnight at 4°C. After washing with Wash Buffer A, the cells were incubated with PLA probes, Anti-Mouse MINUS and Anti-Rabbit PLUS, conjugated to unique oligonucleotides. After the second antibody reaction, the cells were incubated with a Ligation-Ligase solution for 30 min at 37°C and incubated with amplification polymerase solution for 100 min at 37°C. The cells were then washed in Wash Buffer B and stained with Alexa Fluor 594 Phalloidin (Molecular Probes, A12381) for 15 min. The cells were mounted using Vectashield Antifade Mounting Medium with DAPI (Vector Laboratories, Inc., H-1200). PLA signals were detected with a Keyence BZ X-810 fluorescence microscope equipped with a ×60 oil-immersion objective and quantified by ImageJ Fiji software (NIH).

2.14 | siRNA knockdown

Muscle progenitors were cultured in 24-well plates at the density of 5×10^4 cells per well. The next day, the cells were transfected with 10 pmol of siRNA (Invitrogen) using the Lipofectamine RNAiMAX Reagent (Invitrogen) according to the manufacture's protocols. Two days later, the cells were harvested for immunoblot analysis or PLA. Two small-interfering RNA (siRNA) sequences targeted toward STIM1 (Sense strand siRNA: STIM1S-1 5′-GGGAUCUCAGAGGGAUUUGtt-3′, and siSTIM1S-2 5′-CAGAGGGAUUUGACCCAUUtt-3′) were designed using *Silencer* Select (Invitrogen) based on a previously

published report.[28] For ORAI1, one *Silencer* Select Orai1 siRNA (Sense strand siRNA: 5′-GCAACGUGCACAAU CUCAAtt-3′) was used. The *Silencer* Select Negative Control No.1 siRNA (Invitrogen) was used as a negative control.

2.15 | Measurement of ATPase activity

ATPase activity was evaluated as described previously.[29] In brief, cells were homogenized in lysis buffer (0.25 M sucrose, 2 mM Tris–HCl (pH 7.4), 1 mM DTT, and complete protease inhibitor cocktail (Roche)). After a series of centrifugations (800 g for 15 min, 6000 g for 15 min, and 100,000 g for 60 min), the pellet was resuspended in 250 mM sucrose as the microsome fraction. ATP hydrolysis activity of microsomal membranes was measured using a colorimetric ATPase Assay Kit (Abcam) according to the manufacturer's instructions.

2.16 | Statistical analysis

We used R version 4.0.3. For comparison between two groups, unpaired, two-tailed Welch's *t*-test was performed. For more than three groups, Dunnett's or Tukey's multiple comparison test was performed. p Values < 0.05 were considered statistically significant: *$p < 0.05$; **$p < 0.01$; ***$p < 0.001$. N.S., not significant ($p > 0.05$). Data are presented as mean $\pm$ SEM with the mean value of each clone obtained from 2 to 7 experiments. Detailed information on raw data, statistical tests, and p values are provided in the Source Data file (Excel file).

3 | RESULTS

3.1 | Generation of iPS cells from a TAM patient with a frameshift mutation in the CTID coding region of the *STIM1* gene

TAM patient-derived iPS cells were generated from the blood of a TAM patient with a c.1450_1451insGA mutation in the STIM1 gene, a two-base insertion mutation in the C-terminal inhibitory domain (Figure 1A).[15] Three clones with high proliferative potential and pluripotency (TAM#4, TAM#9, and TAM#11) were selected for this study. Each clone formed iPSC-like colonies (Figure 1B), had a normal karyotype (46, XY), expressed OCT3/4, NANOG, and SOX2, and formed teratomas in immunodeficient NOD-Scid mice (Figure S1A–E). Sanger sequencing confirmed that the TAM patient-derived iPSCs
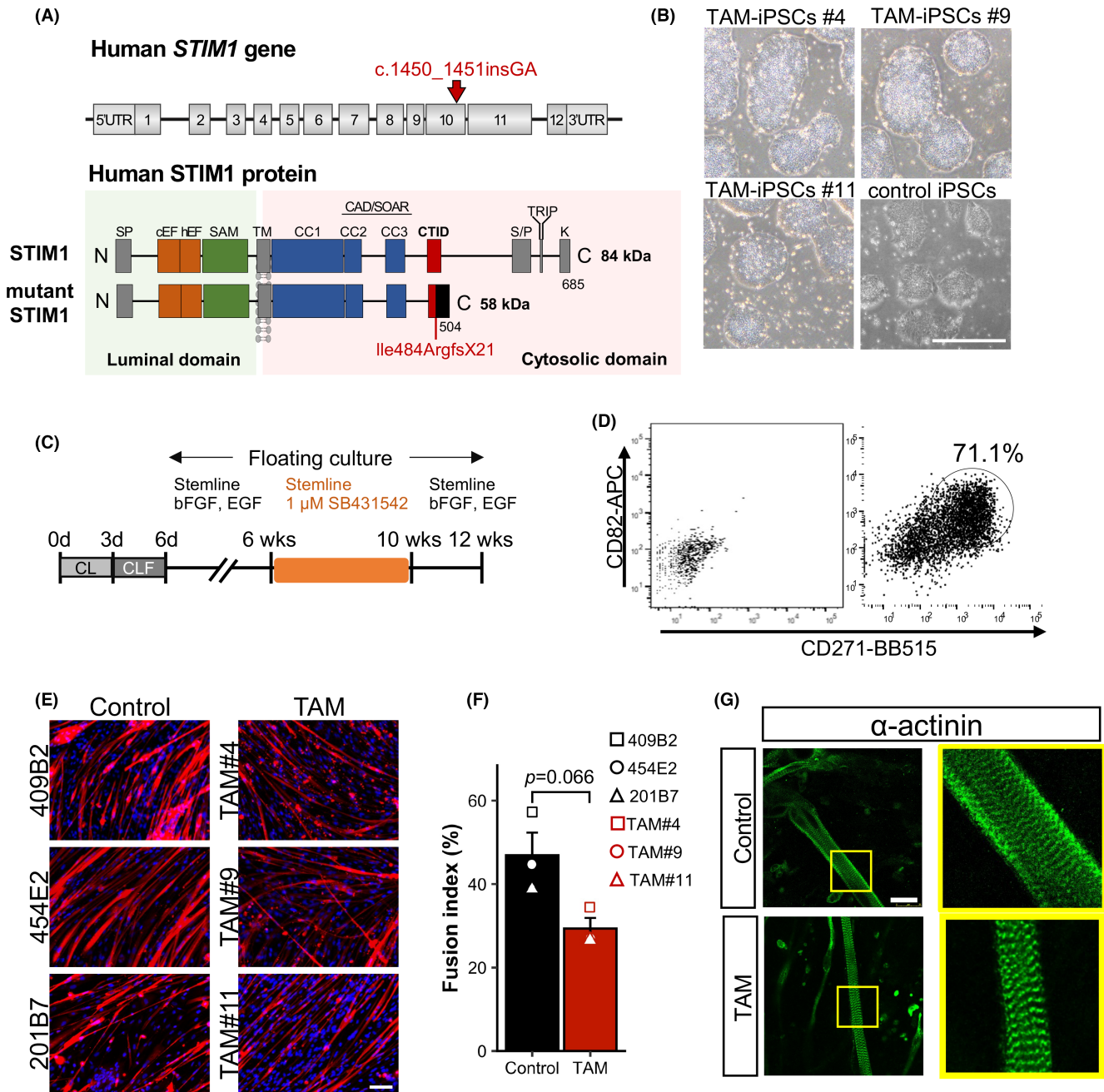
FIGURE 1 Derivation of skeletal muscle progenitors from control and TAM-iPSCs. (A) The structures of the *STIM1* gene and STIM1 protein of the patient. The TAM patient has an autosomal dominant mutation (c1450_1451insGA; p. Ile4584ArgfsX21) in the C-terminal inhibitory domain (CTID). CAD/SOAR, channel-activating domain/the STIM/ORAI activating region; CC1, conserved cytosolic coiled-coil domain 1; CC2, conserved cytosolic coiled-coil domain 2; CC3, conserved cytosolic coiled-coil domain 3; cEF, canonical EF-hand motif; hEF, hidden EF-hand motif; K, Lys-rich domain; S/P, Pro/Ser-rich domain; SAM, sterile α-motif; SP, signaling peptide; TM, transmembrane; TRIP, Thr-Arg-Ile-Pro sequence. (B) Phase contrast images of TAM-iPSCs (TAM#4, TAM#9, and TAM#11) and control-iPSCs (409B2) colonies on feeder-free iMatrix511-coated dishes. Scale bar = 500 μm. (C) Schematic description of a new protocol for induction of skeletal muscle progenitors. Detailed protocol is described in Materials and Methods. C: CHIR-99021, L: LDN-193189, F: bFGF. (D) Representative plot of flow cytometry of iPSC-derived myogenic cells. CD82$^+$/CD271$^+$ double positive cells were sorted as skeletal muscle progenitors. (E) Representative images of myotubes formed by muscle progenitors derived from control-iPSCs (409B2, 454E2, and 201B7) and TAM-iPSCs (TAM#4, TAM#9, and TAM#11). Scale bar = 100 μm. (F) Fusion index of (E). Experiments were performed 4 times. Data are mean ± SEM with the averaged value of each clone. Welch's *t*-test (two-tailed). (G) α-Actinin staining of myotubes (Control: 409B2, TAM: TAM#4) formed after 1-week culture in differentiation medium. Right panels are enlarged images of the yellow squares in the left panels. Scale bar = 25 μm.

retained the parental two-base insertion at CTID in the STIM1 gene in one allele (Figure S1F).

3.2 | Derivation of skeletal muscle progenitors from patient iPSCs

Previously, we reported a modified EZ sphere method for induction of skeletal muscle progenitors from human iPSCs.[22] A recent study showed that longer cultures are necessary to induce skeletal muscle cells in the later developmental stage.[30] Therefore, we prolonged the induction period from 6 to 12 weeks (Figure 1C). Myogenic progenitors grew more slowly than non-myogenic cells (data not shown). To avoid loss of myogenic cells during the long induction process, we investigated several culture conditions and found that removal of FGF2 (bFGF) and EGF from the culture medium in a later step (6–10 weeks) significantly enriched PAX7-positive myogenic progenitors (Figure S2). After 12 weeks induction culture, we sorted CD271$^+$CD82$^+$ cells[31] as muscle progenitors by flow cytometry (Figure 1D) and cultured them in a differentiation medium. We induced myogenic cells from three TAM-iPS cells (TAM#4, TAM#9, and TAM#11) and control iPS cells from a healthy donor (409B2, 454E2, and 201B7).[17–19] The fusion index (numbers of nuclei in myotubes/total nuclei × 100 (%)), a commonly used quantitative metric to assess myogenesis, for TAM-iPSC-derived myogenic cells tended to be lower than that of control ones, although there was no statistical significance (Figure 1E,F). Both control and TAM-derived myotubes spontaneously contracted (Videos S1 and S2) and showed a sarcomere-like structure when immunostained with an anti-α-actinin antibody (Figure 1G). No significant difference was observed in the expression of myosin heavy chain isotypes (MYH1, MYH2, MYH3, MYH7, and MYH8) between TAM and control myotubes (Figure S3).

3.3 | STIM1 and ORAI1 mRNA levels were maintained but protein levels were reduced in TAM iPSC-derived myotubes

To assess whether myotubes induced from patient-iPSCs can be used for in vitro disease modeling of TAM, the expressions of STIM1, ORAI1, RYR1, SERCAs (SERCA1a, SERCA1b, SERCA2a, SERCA2b), and calsequestrin 1 (CASQ1) were examined by RT-qPCR (Figure 2A; Figure S3). STIM1 and ORAI1, molecules responsible for SOCE, and RyR1, a Ca^{2+} release channel in the ER/SR membrane, were expressed at almost the same level in myotubes from control-iPSCs and TAM-iPSCs. In general, when a premature stop codon (PTC) was located within 50–55 nt upstream of the exon junction of the most 3′ side, nonsense-mediated mRNA

decay (NMD) did not occur.[32,33] The mutated STIM1 seems to evade NMD, because the premature stop codon locates 31 nt upstream of the exon 11 and exon 12 junction (the exon junction of the most 3′ side; Figure S4). SERCA1b (fetal type) was abundantly expressed in iPSC-derived myotubes, but the mRNA level of SERCA1a (adult fast type) was around one-twentieth of that of adult skeletal muscle tissue. This expression pattern was also found in myotubes formed by primary myoblasts (data not shown), indicating that myotubes formed in culture are not fully matured. Interestingly, CASQ1 a major Ca^{2+}-binding protein in the SR tended to be upregulated in TAM myotubes, although there was no statistically significant difference (Figure S3).

Next, we assessed the STIM1 and ORAI1 protein expression by immunoblotting. An antibody recognizing the N-terminus of STIM1 revealed that myotubes derived from TAM-iPSCs expressed a long splice variant of STIM1 with an extended C-terminal domain (STIM1-L; 115 kDa),[28] STIM1 (84 kDa), and a truncated, disease-causing STIM1 (58 kDa; Figure 2B; Figures S5 and S6). The STIM1 protein level was reduced to approximately 30% of the control level (Figure 2C). On ORAI1 blotting, the band appeared broad due to the glycosylation of ORAI1 (Figure 2B).[34,35] There was no difference in the ORAI1 protein level between control and TAM myotubes (Figure 2C).

3.4 | c.1450_1451insGA mutation altered subcellular localization of STIM1 in TAM iPSC-derived myotubes

Okuma et al.[15] reported that overexpression of mutant STIM1 (c.1450_1451insGA) in C2C12 cells resulted in accumulation of STIM1 around nuclei and exhibited an aggregation-like appearance in shrunken cytoplasm. In control iPSC-derived myotubes, the STIM1 signals were distributed in the cytoplasm, but the signals were only weakly detected in the patient iPSC-derived myotubes (Figure 2D; Figure S7). On the contrary, ORAI1 signals were distributed in the cytoplasm and not decreased on the immunofluorescent images of patient-iPSC-derived myotubes (Figure 2D).

3.5 | TAM iPSC-derived myotubes had low Ca^{2+} levels in both cytoplasm and ER/SR in a resting state and showed blunted SOCE

The STIM1 mutation (p. Ile484ArgfsX21) is reported to show impaired SOCE when overexpressed in C2C12 cells or HEK293 cells.[15] To examine SOCE in iPSC-derived myotubes, first we depleted Ca^{2+} from the extracellular fluid (0 mM Ca^{2+}; Figure 3A–C). In the second experiment, we
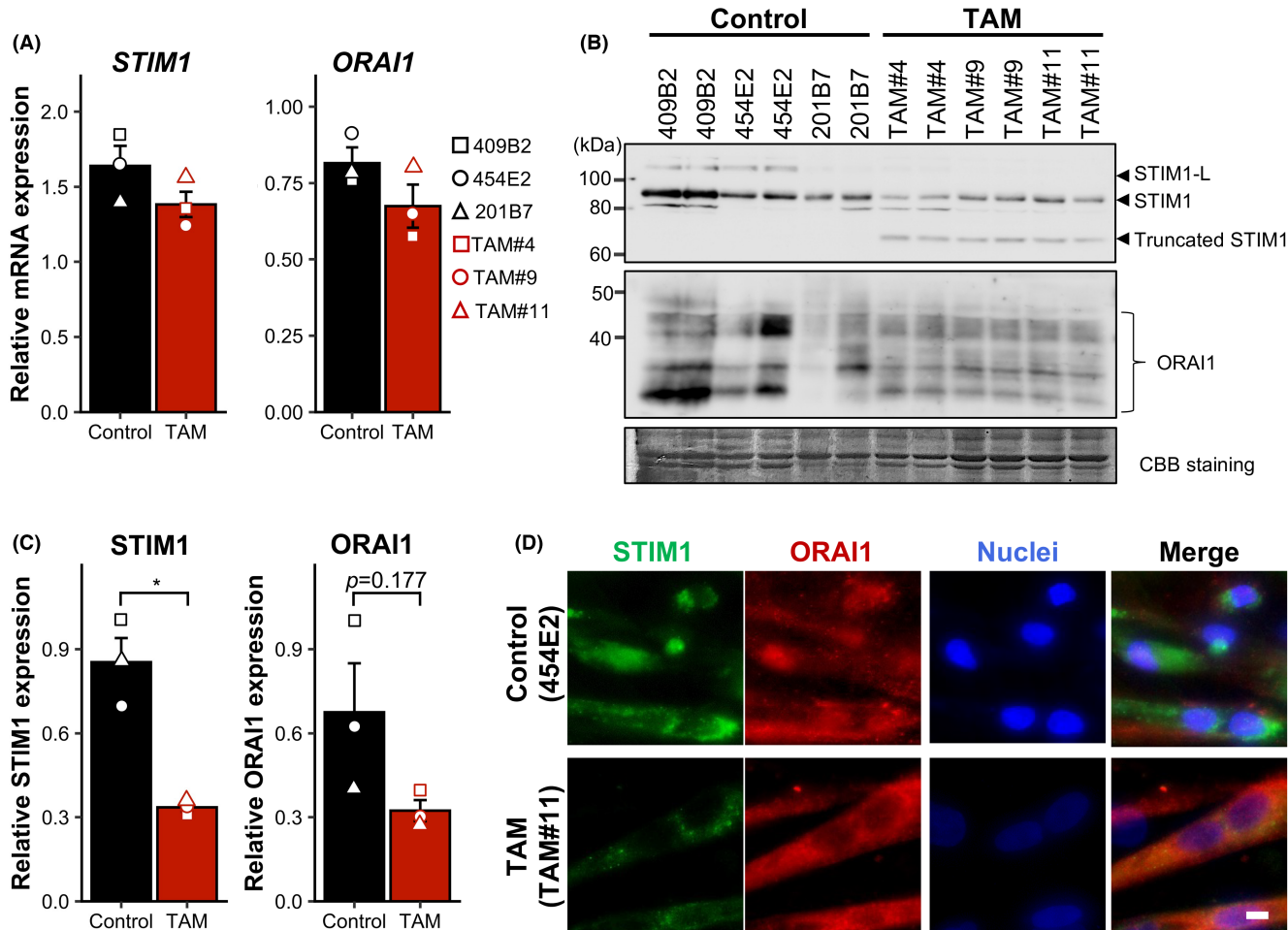
FIGURE 2 STIM1 protein level was reduced, and the subcellular localization of STIM1 was altered in TAM myoblasts. (A) RT-qPCR analysis of *STIM1* and *ORAI1* in myotubes differentiated from control iPSCs (409B2, 454E2, and 201B7; black columns) and TAM-iPSCs (TAM#4, TAM#9, and TAM#11; red columns). The STIM1 primers amplify both normal and mutated transcripts. The experiment was performed 3–7 times. (B) Immunoblot analysis using a STIM1 antibody recognizing the N-terminus of STIM1 (B) and anti-ORAI1 antibody (C) from control iPSCs and TAM-iPSCs. CBB staining is shown as a loading control. (C) Quantification of the signal intensities of STIM1 (left) and ORAI1 (right). Sample preparations and immunoblotting were performed four times. (D) Representative confocal images of control (454E2) and TAM#11 myotubes stained with anti-STIM1 antibody recognizing the N-terminus of STIM1 (BD 610954). Scale bar = 25 μm. Uncropped images of B, and negative controls (siRNA experiments) are shown in Figure S6. Data are mean ± SEM with the average value of each clone. Two-tailed Welch's *t* test.

FIGURE 3 TAM myotubes show lower levels of cytosolic Ca^{2+} and shortage of Ca^{2+} in ER/SR compared with controls, and show blunted SOCE. (A) Representative recording of cytosolic Ca^{2+} changes induced by perfusing 2 mM Ca^{2+} and 0 mM Ca^{2+} solutions on control (454E2, black, 12 cells) and TAM (TAM#11, red, 24 cells) myotubes. Data are mean ± SEM. Myotubes derived from control and TAM iPSCs were loaded with Fura-2/AM to monitor changes in cytosolic Ca^{2+} concentration. (B) Comparison of the resting cytosolic Ca^{2+} in A. (C) Maximal cytoplasmic Ca^{2+} rise after re-addition of 2 mM Ca^{2+}. (D) Representative cytosolic Ca^{2+} change by treatment of thapsigargin in control (454E2, black, 12 cells) and TAM (TAM11, red, 12 cells) myotubes. Data points are mean ± SEM. (E) Comparison of the resting cytosolic Ca^{2+} in D. (F) The maximal cytoplasmic Ca^{2+} rise after addition of 2 mM Ca^{2+} with 5 μM thapsigargin. In A–F, the experiment was performed three times. More than 10 cells were recorded per clone in each experiment. (G) Cartoon to explain experiments in H-L. Myotubes were lentivirally transduced with rCEPIA1er, an ER/SR-specific Ca^{2+} indicator. (H) Trace showing rises in cytosolic Ca^{2+} induced by Ca^{2+} release from the ER/SR by exposure to 50 mM caffeine. (Control: 22 cells, TAM#9: 26 cells). (I) The Ca^{2+} release to the cytoplasm, the range of F_{340}/F_{380} elevation from no caffeine (basal) to 50 mM caffeine (peak), in H. (J) Comparison of the CEPIA intensity in each myotube at a resting state. More than 20 cells per experiment (2–3 experiments). (K) Trace showing changes in the ER/SR Ca^{2+} induced by 50 mM caffeine in control (black, 22 cells) and TAM myotubes (red, 26 cells). Values were normalized to F_0. (L) Ca^{2+} reduction of the ER/SR, the range of F/F_0 depression from no caffeine to 50 mM caffeine addition in K. Experiments were performed twice (3 times for 201B7). In each experiment, more than 20 cells/clone were recorded and averaged. Data are mean ± SEM with the average value of each clone. Two-tailed Welch's *t*-test.
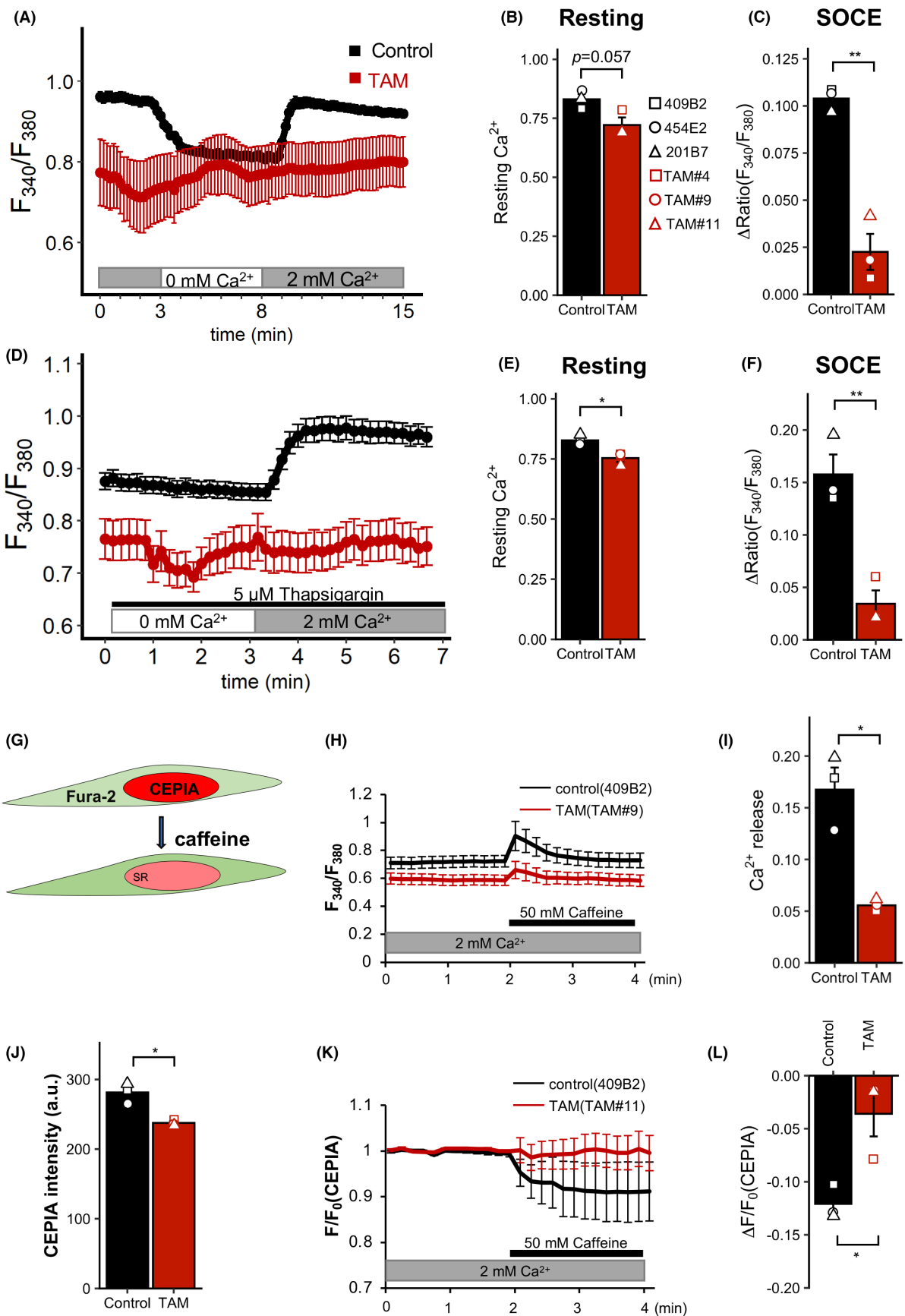
added a SERCA inhibitor, thapsigargin (Figure 3D–F). The cytoplasmic Ca^{2+} level was monitored using Fura-2/AM. Importantly, resting $[Ca^{2+}]$ levels, the mean value of F_{340}/F_{380} within the first minute of the experiment, were lower in TAM myotubes than in control myotubes (Figure 3A,B,D,E). In both experiments, the elevation of the cytoplasmic Ca^{2+} evoked by Ca^{2+} depletion was almost undetectable in TAM myotubes in all three TAM clones tested (Figure 3A,C,D,F).

Next, cytoplasmic Ca^{2+} level and Ca^{2+} stores in ER/SR were simultaneously monitored using rCEPIA1er,[36] an ER-specific Ca^{2+} indicator, and Fura-2/AM (Figure 3G). Caffeine was used to stimulate RyR1-mediated Ca^{2+} release from ER/SR. Compared with controls, caffeine had less effect on the elevation of cytosolic Ca^{2+} in TAM myotubes (Figure 3H,I). In the resting state, TAM myotubes showed a slightly lower intensity of rCEPIA1er signals than the control, suggesting less Ca^{2+} storage in ER/SR (Figure 3J). The decrease in fluorescence intensity of rCEPIA1er in ER/SR after caffeine treatment was smaller in the TAM myotubes than in control myotubes (Figure 3K,L). The results suggested that the TAM myotubes in a resting state had lower Ca^{2+} concentrations in both the cytoplasm and ER/SR compared to the control myotubes.

3.6 | Antioxidants rescued SOCE of TAM myotubes

Dysregulation of intracellular Ca^{2+} causes oxidative stress and ER stress, which further impair Ca^{2+} handling in muscular disorders.[37] Therefore, we next tested the effects of two well-characterized free radical scavengers, MCI-186 (Edaravone), and NAC (N-acetyl-L-cysteine) on SOCE in the TAM myotubes (Figure 4A). Antioxidants did not improve the fusion index in TAM myotubes (Figure 4B,C). Importantly, the two antioxidants significantly restored SOCE of TAM myotubes to the control level (Figure 4E).

Caffeine-induced Ca^{2+} release from the ER/SR tended to be increased by the antioxidants, although there was no statistically significant difference (Figure 4F,G; Figure S8). Interestingly, untreated TAM myotubes responded poorly to caffeine, compared with controls ($\Delta F_{340}/F_{380} > 0.03$ was judged as "responded"). NAC treatment ($p = 0.024$) or MCI-186 ($p = 0.052$) increased the percentage of responders in TAM myotubes (Figure 4I). On the contrary, MCI-186 or NAC did not improve SOCE in control iPSC-derived myotubes (Figure S9). The antioxidants showed a tendency to increase the ATPase activity of SERCA in TAM myotubes, although not statistically significantly (Figure S8).

3.7 | Antioxidant treatment improved STIM1-ORAI1 interaction in TAM myotubes

To understand the mechanisms by which antioxidants rescued SOCE, the levels of STIM1 and ORAI1 proteins in TAM myotubes were examined. The antioxidants did not increase the expression of STIM1 and ORAI1 (Figure 5A–C). The interaction of STIM1 and ORAI1 after induction of SOCE was examined by a proximity ligation assay (PLA). PLA signals of myotubes were increased by antioxidants, but there was no statistically significant difference between untreated and antioxidant-treated TAM myotubes, due to the much larger number of signals in the control (Figure 5D,E).

3.8 | TAM myotubes are vulnerable to H_2O_2 treatment

The augmentation of SOCE by antioxidants in TAM myotubes suggested increased oxidative stress in TAM myotubes. To test this hypothesis, we examined ROS levels in control and TAM myotubes using H2DCFDA. The levels were unexpectedly low in TAM myotubes (Figure S10A). Oxyblots revealed no clear difference in protein oxidation levels between control and TAM myotubes (Figure S10B–E). Importantly, TAM myotubes were more sensitive to H_2O_2 than control myotubes (Figure S10F–H). These results suggest the possibility that protective mechanisms against free radicals are not fully functional in TAM myotubes.

3.9 | Antioxidant treatment restored SOCE via upregulation of BiP, a major ER chaperone

In the skeletal muscle of TAM patients, a honeycomb-like tubular structure is observed by electronic microscopy, which resembles the stacked ER cisternae observed in cells under ER stress.[38] Therefore, the restoration of SOCE by antioxidants suggested that antioxidants reduced ER stress in TAM myotubes. To examine whether reduction of ER stress by antioxidants improved SOCE, we evaluated the expression of ER stress-related proteins (BiP, PDI, IRE1α, PERK, ATF-6, ATF-4, CHOP, and XBP-1) by immunoblotting. BiP, an ER Hsp70 chaperone, and PDI, a family of protein disulfide isomerases, that play important roles in ER quality control and repair of misfolded proteins. These two molecules were abundantly detected in myotubes (Figure 6A). Unexpectedly, the expression of
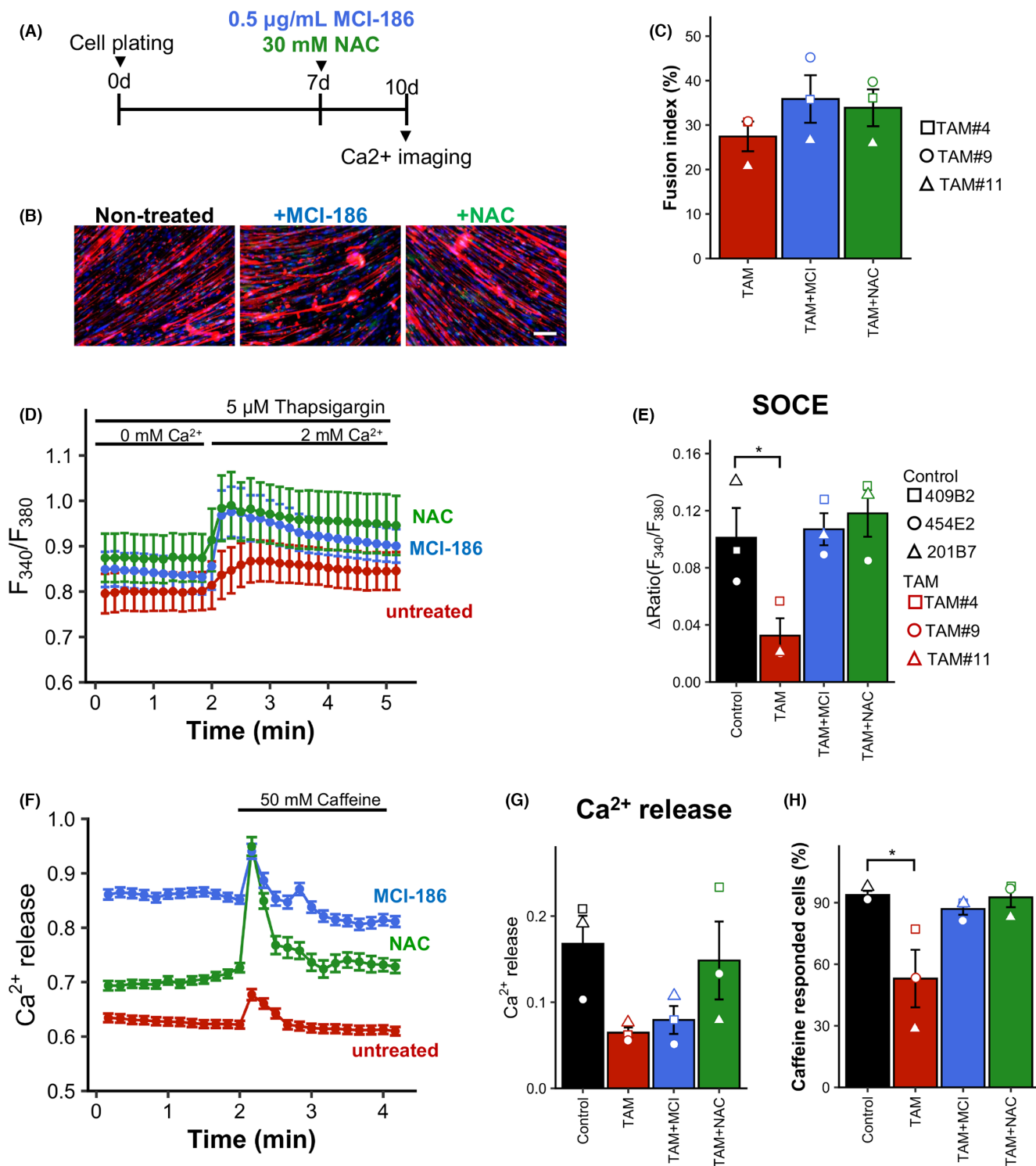
FIGURE 4 Antioxidants NAC and MCI-186 restored SOCE in TAM patient-iPSC-derived myotubes. (A) Experimental design of antioxidant treatment. Myotubes formed 7 days after plating were treated with 0.5 μg/mL MCI-186, 30 mM NAC for 3 days. (B) Representative images of myotubes stained for MYHC (MF20, red), MYOGENIN (green), and DAPI (nuclei, blue) after antioxidant treatment. Scale bar = 100 μm. (C) Fusion index. The mean value of each clone was obtained from 2 to 3 experiments. SR Ca^{2+} depletion was induced by thapsigargin (5 μM). Intracellular Ca^{2+} of TAM-derived myotubes was measured by Fura-2/AM. (D) Comparison of the SOCE value in control and TAM myotubes in D. SOCE value was calculated as 2 mM Ca^{2+} peak – 0 mM Ca^{2+} base. (E) Representative recording of Ca^{2+} release to the cytoplasm by 50 mM caffeine in TAM#4-myotubes treated with 0.5 μg/mL MCI-186 (blue, 30 cells), 30 mM NAC (green, 30 cells), and untreated control (black, 27 cells). (F) The maximal cytoplasmic Ca^{2+} rise after addition of 50 mM caffeine. (G) Percentage of myotubes that responded to caffeine ($\Delta F_{340}/F_{380} > 0.034$). More than 40 myotubes per group were analyzed and averaged. Experiments (D–H) were repeated twice (three times for 201B7). Data are the mean of three clones ± SEM with the average value of each clone. Dunnett's test versus untreated TAM myotubes (C), or versus control myotubes (E, G, and H). *$p < 0.05$.
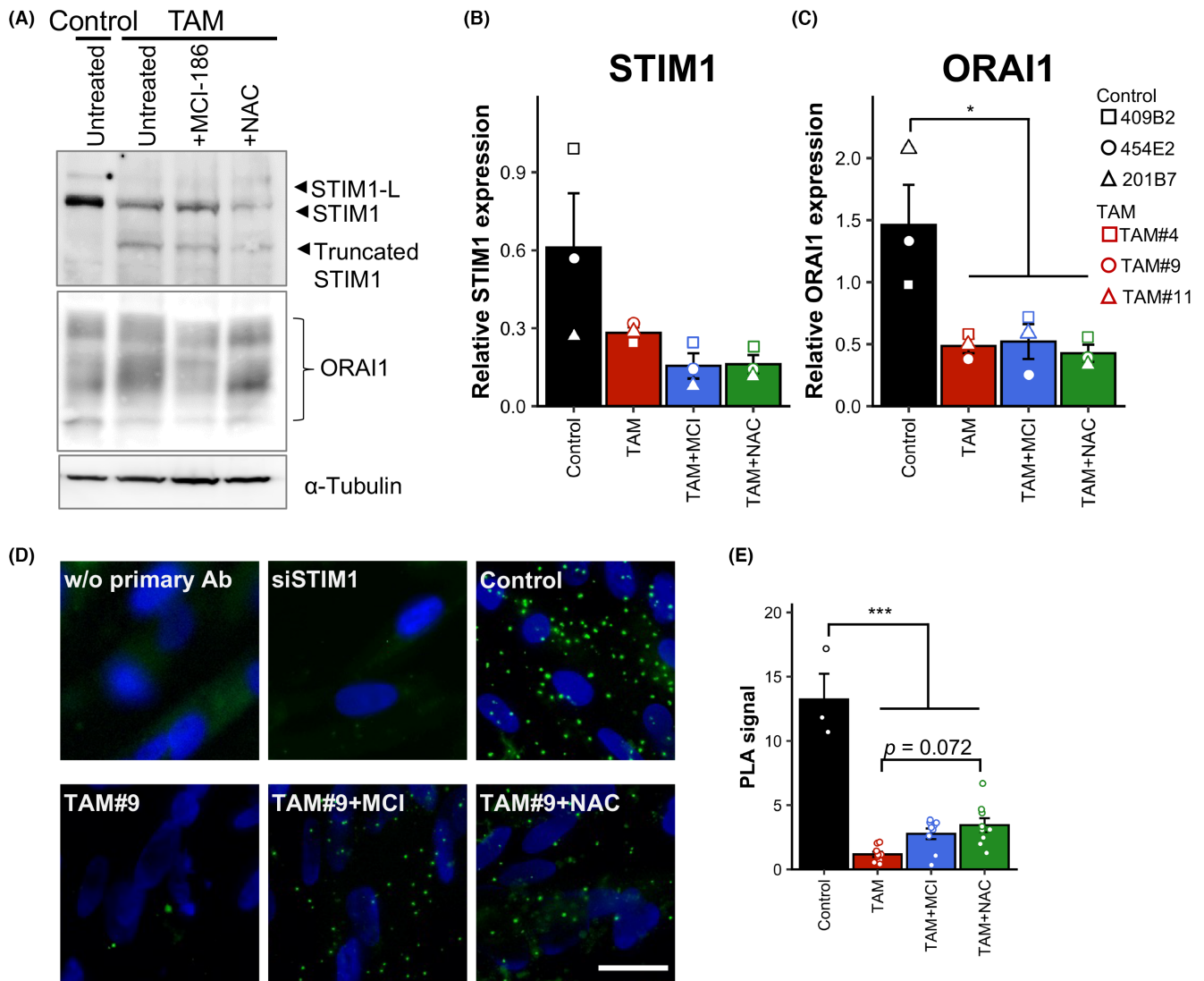
FIGURE 5 Antioxidants improved STIM1/ORAI1 interaction in a Ca^{2+} store-depleted condition in TAM myotubes (A) Representative immunoblot with an antibody recognizing the N-terminus of STIM1 and anti-ORAI1 antibody of extracts from untreated and antioxidants (0.5 µg/mL MCI-186 or 30 mM NAC)-treated control and TAM-iPS derived myotubes. α-Tubulin was used as a loading control. (B and C) Signal intensities of STIM1 (B) and ORAI1 (C) normalized to those of untreated myotubes. The experiment was repeated 2–6 times. Data are mean ± SEM with the average value of each clone. In B and C, p values were calculated using Dunnett's test (vs. control). *$p < 0.05$. (D) Representative PLA images of control (454E2) and TAM myotubes (TAM#9) after induction of SOCE using thapsigargin. The PLA signals (green fluorescent dots) indicate the proximity of STIM1 and ORAI1. Scale bar = 25 µm. Images without primary antibodies and with siRNAs siSTIM1 are shown as negative controls. (E) Quantification of fluorescent dots/cell in control (454E2) myotubes, and untreated, MCI-186-treated-, or NAC-treated TAM myotubes (TAM#4, TAM#9, TAM#11). PLA assay was performed three times. Data are mean ± SEM with the average value of each clone. Tukey's multiple comparisons test: *$p < 0.05$; ***$p < 0.001$.

BiP was suppressed in TAM myotubes but significantly restored by antioxidant treatment (Figure 6B). PDI was not increased by antioxidants (Figure 6C). PKR-like endoplasmic reticulum kinase, PERK, was not found to be expressed differently in TAM and control myotubes (Figure S11). The expression of other ER stress-related markers, IRE1α, ATF-6, ATF-4, CHOP, and XBP-1, was all below the detection limit (data not shown), questioning the presence of ER stress in TAM myotubes. Based on these results, we hypothesized that the antioxidants rescued SOCE in TAM myotubes by upregulating BiP.

To test the hypothesis, we examined the effects of BiP Inducer X (BIX) on SOCE in TAM myotubes. BIX activates transcription of the BiP gene in a dose-dependent manner.[39] Interestingly, the BIX treatment of TAM myotubes for 4 days greatly improved SOCE, whereas it did not augment SOCE in control myotubes (Figure 6D,E). Caffeine-induced Ca^{2+} release from ER/SR in TAM myotubes
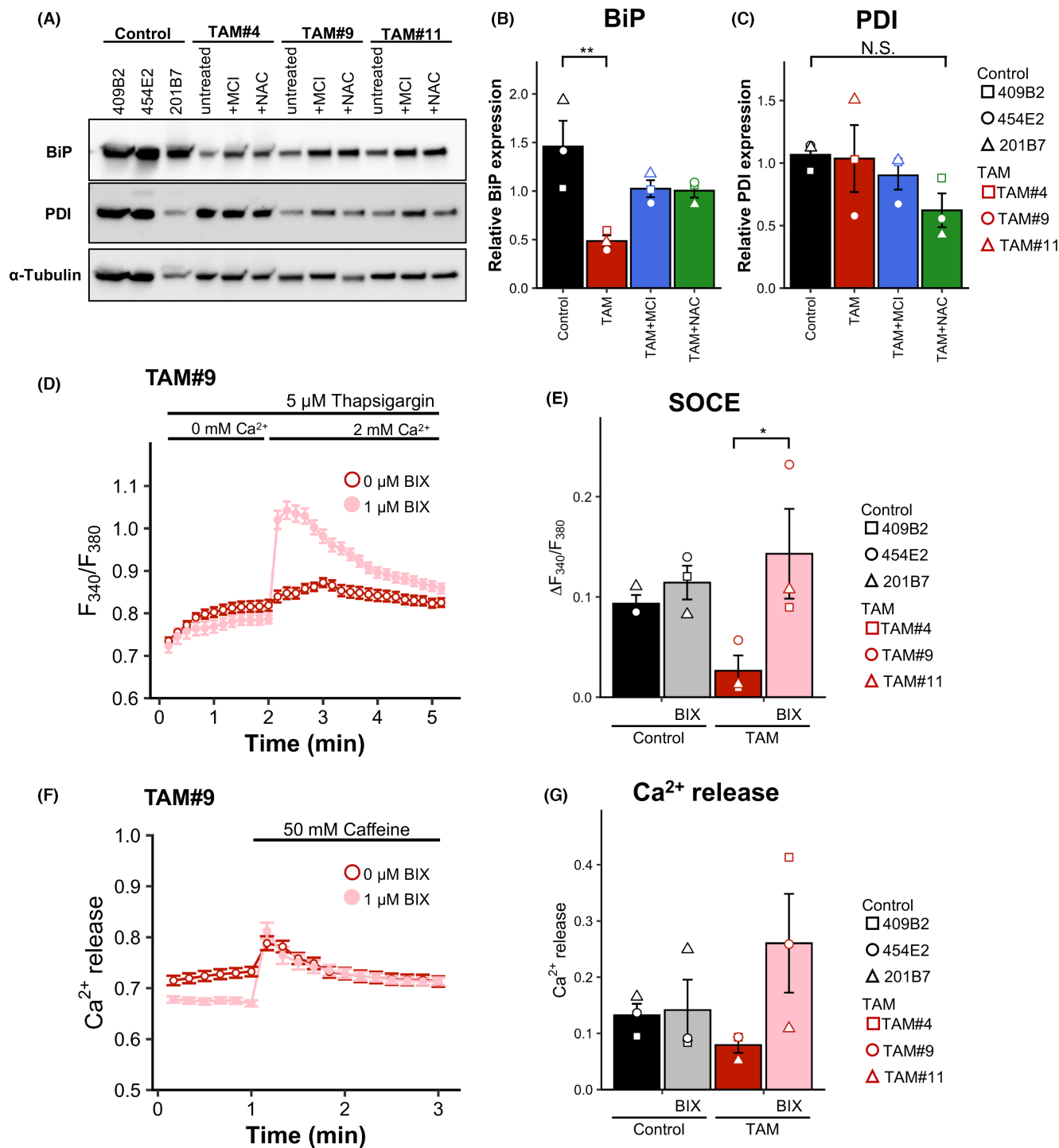
FIGURE 6 Antioxidants upregulated BiP, and an inducer of BiP restored SOCE in ER/SR of TAM myotubes. (A) Representative immunoblots of BiP and PDI in control (409B2, 454E2, and 201B7) and TAM myotubes (TAM#4, TAM#9, and TAM#11) treated with antioxidants (0.5 μg/mL MCI-186 or 30 mM NAC). α-Tubulin is shown as a loading control. (B and C) Quantification of A. The expressions of BiP (B) and PDI (C) were normalized to those of 409B2 myotubes. Sample preparation and immunoblotting were repeated 2–4 times for each clone, and the average value of each clone was plotted. Dunnett's test (vs. control myotubes). **$p < 0.01$, N.S. = not significant. (D) Representative recording of cytoplasmic Ca^{2+} changes induced by 5 μM thapsigargin in TAM#9-myotubes treated with 1 μM (pink circle, 30 cells) and 0 μM (red circle, 22 cells) BiP inducer X (BIX). (E) Maximal cytoplasmic Ca^{2+} rise after addition of 2 mM Ca^{2+} with 5 μM thapsigargin in TAM myotubes (TAM#4, TAM#9, and TAM#11). Myotubes were treated with or without 1.0 μM BIX. (F) Representative recording of Ca^{2+} release to the cytoplasm by 50 mM caffeine in TAM#9 myotubes treated with 1 μM (pink circle, 24 cells) and 0 μM (red circle, 22 cells) BIX. (G) Ca^{2+} release (ΔF340/F380 (peak-basal)) evoked by 50 mM caffeine in TAM myotubes (TAM#4, TAM#9, and TAM#11). Myotubes were treated with or without 1.0 μM BIX. The experiment was performed more than twice, and the average value of each clone was plotted. In E and G, Tukey's multiple comparison test was performed. *$p < 0.05$.

tended to be increased by BIX, although the difference was not statistically significant (Figure 6F,G).

4 | DISCUSSION

We generated iPS cells from a TAM patient with a rare mutation (p.Ile484ArgfsX21) in the *STIM1* gene and induced myogenic cells using our new 12-week-floating culture method. Growth factor-free culture medium drastically enriched PAX7-positive muscle progenitors (Figure S2). Our new protocol is applicable to a wide-range of muscle diseases.

Our TAM-iPSC-derived myotubes showed severely reduced SOCE and deficiency in Ca^{2+} stores in the ER/SR (Figure 3A–F). This result is consistent with a previous report by Okuma et al.[15] using C2C12 cells or HEK293 cells overexpressing the mutant STIM1. Immunostaining showed poor expression of STIM1 protein in the cytoplasm of TAM-iPSC-derived myotubes (Figure 2D). Immunoblotting analysis showed lower levels (30% of the controls) of STIM1 protein in patient-iPSC-derived myotubes than in control myotubes (Figure 2B,C). Our PLA assay demonstrated that STIM1 does not efficiently interact with ORAI1 on Ca^{2+} depletion in ER/SR in patient muscle, but antioxidants partially restored the interaction (Figure 5D,E).

The mutation of the patient we analyzed is a heterozygous insertion mutation of *STIM1* gene, c.1450_1451insGA, which results in a frameshift and generates a premature stop codon (p.Ile484ArgfsX21). $STIM1^{I484R}$ resides in the cytosolic CTID domain, and the mutant protein lacks the downstream residues of STIM1 including the C-terminal part of CTID, S/P, and K domains (Figure 1A). The K domain, also known as the polybasic domain, interacts with phospholipids in plasma membrane (PM), concentrates STIM1 at ER-PM junctions, and improves the efficiency with which STIM1 interacts with ORAI1.[40–42] Therefore, whereas the K domain is reported to be not absolutely necessary for SOCE in overexpression studies, it may be more critical at endogenous protein levels, in which individual STIM1 may be too sparse to effectively interact with ORAI1.[42] STIM1 is present as a dimer and oligomerizes upon Ca^{2+} depletion. The TM domain as well as the CC1 and CC3 domains contribute to the oligomerization.[43,44] Because the $STIM1^{I484R}$ mutant possesses these domains and the mutant protein is expressed at a comparable level to the wild-type protein (Figure 2B), it is expected that the mutant STIM1 is incorporated into the STIM1 oligomers at a similar ratio to that of the wild-type protein. Thus, the reduction of approximately 70% in STIM1 protein levels in TAM myotubes (Figure 2B,C)

may be partly due to the instability and degradation of STIM1 dimers including truncated STIM1. In addition, structurally defective STIM1 is thought to destabilize the STIM1/ORAI1 complex at the plasma membrane. Because antioxidants cannot correct the structural defect of the truncated STIM1, it is reasonable that antioxidants only partially restored the STIM1/ORAI1 interaction in the TAM myotubes. Therefore, how antioxidants significantly improved SOCE in the TAM myotubes without upregulating STIM1 expression is unclear and needs further investigation.

Recently, Kim et al.[16] reported that the same $STIM1^{I484R}$ mutation (p.Ile484ArgfsX21) augmented ORAI1 channel function and hypothesized that the mutant STIM1 protein can interact with ORAI1 more efficiently than wild-type STIM1. However, their conclusion is based on experiments in which YFP-STIM1 (wild-type or mutant) and mCherry-ORAI1 were overexpressed in HEK-293T cells or primary myoblasts, and these may not fully mimic the skeletal muscle of the patient. In sharp contrast, we utilized myotubes differentiated from iPSCs derived from the $STIM1^{I484R}$ patient. These cells are expected to express both the wild-type and mutant STIM1 together with the wild-type ORAI1 at a physiologic level very close to the patient's skeletal muscle, and therefore provide a good disease model to gain deeper mechanistic insight into the pathogenesis of the mutation.

Tubular aggregate myopathy is usually associated with gain-of-function mutations in the *STIM1* or *ORAI1* gene.[7–12] However, tubular aggregates are known to form in many conditions. Tubular aggregates were first described in patients with periodic hypokalemic paralysis,[45] and later in several pathological conditions such as inflammatory myopathy, malignant hyperthermia, congenital myasthenic syndromes, alcohol myopathy, prolonged anoxia, diabetes, and endocrine disorders.[14] Chronic inhibition of the mitochondrial ATP synthesis also facilitates formation of tubular aggregates.[46] Interestingly, tubular aggregates also develop in type-IIB fibers of physiologically aging male mice.[47–49] Therefore, tubular aggregate formation is not specific to the constitutive activation of Ca^{2+} entry caused by gain-of-function mutations in the *STIM1* or the *ORAI1* gene, and it is possible that the chronic disruption of Ca^{2+} homeostasis observed in our patient also caused the tubular aggregate formation.

In the present study, we showed that antioxidants restored SOCE in TAM myotubes via restoration of BiP expression. The mechanisms by which the BiP protein level was reduced in TAM myotubes and how antioxidants upregulated BiP remain to be determined. For the restoration of SOCE by BiP, one possibility is that BiP improved the folding of STIM1 protein and its proper distribution, thereby restoring interaction with ORAI1. Interestingly,

the affinity of BiP to unfolded proteins is reported to be decreased in low Ca^{2+} conditions,[50] suggesting that restored SOCE and Ca^{2+} stores in the ER/SR further augmented BiP function. In addition to its chaperone function, BiP serves as a high-capacity Ca^{2+}-binding protein to store Ca^{2+} in the ER and is involved in regulation of Ca^{2+} homeostasis.[51–53] Therefore, restoration of BiP might also improve Ca^{2+} handling in TAM myotubes.

There was no clear difference in the intracellular ROS levels and the levels and patterns of oxidative proteins in a resting state between control and TAM myotubes (Figure S10). These observations do not support our original hypothesis that a deficiency of Ca^{2+} stores in ER/SR causes oxidative stress and impairs SOCE in TAM myotubes. Intriguingly, however, TAM myotubes showed decreased cell viability compared to control myotubes in low H_2O_2 concentrations (Figure S10). These observations suggest that TAM myotubes are vulnerable to low levels of ROS, and that BiP recovery by antioxidants restored the resistance of TAM myotubes to ROS. Thus, the vulnerability of TAM myotubes to ROS might be a major contributor to the pathogenesis of TAM.

In summary, we optimized the protocol to induce muscle progenitor cells from human iPSCs and established an in vitro disease model for TAM caused by a rare mutation (p. Ile484ArgfsX21). Our analysis showed that SOCE was severely impaired in the TAM myotubes, and antioxidants significantly rescued the defect mainly by restoring the expression of the major ER chaperone BiP. Therefore, besides antioxidants, restoration of BiP expression and function by low molecular weight compounds is a potential therapeutic tool for TAM with low SOCE.

AUTHOR CONTRIBUTIONS
Fusako Sakai-Takemura and Yuko Miyagoe-Suzuki performed the experiments and analyzed the data. Fusako Sakai-Takemura, Fumiaki Saito, Kiichiro Matsumura, and Yuko Miyagoe-Suzuki designed the study, wrote the manuscript, and prepared the figures. Ken'ichiro Nogami, Ahmed Elhussieny, and Yusuke Maruyama provided technical support and discussed the results weekly. Yoshitsugu Aoki, Shin'ichi Takeda, and Yuko Miyagoe-Suzuki supervised and coordinated the project. All authors approved the final manuscript.

ACKNOWLEDGMENTS
We thank all members in Department of Molecular Therapy for discussion and encouragement.

CONFLICT OF INTEREST STATEMENT
The authors declare no conflicts of interest.

DATA AVAILABILITY STATEMENT
Data generated during this study and detailed protocols are available from the corresponding author on request.

ETHICAL STATEMENT
All experimental procedures were approved by the Ethical Committee of the National Institute of Neuroscience, National Center of Neurology and Psychiatry (NCNP), Japan, and performed according to the guidelines. We obtained written informed consent from the TAM patient before starting the project.

ORCID
Fusako Sakai-Takemura https://orcid.org/0000-0003-0509-0343
Fumiaki Saito https://orcid.org/0000-0002-5532-6193
Ahmed Elhussieny https://orcid.org/0000-0002-1192-5282
Kiichiro Matsumura https://orcid.org/0000-0002-5237-8430
Shin'ichi Takeda https://orcid.org/0000-0003-4780-6290
Yoshitsugu Aoki https://orcid.org/0000-0002-9038-7506
Yuko Miyagoe-Suzuki https://orcid.org/0000-0001-8458-6237

REFERENCES
1. Liou J, Kim ML, Heo WD, et al. STIM is a Ca^{2+} sensor essential for Ca^{2+}−store-depletion-triggered Ca^{2+} influx. *Curr Biol*. 2005;15(13):1235-1241.
2. Stathopulos PB, Li GY, Plevin MJ, Ames JB, Ikura M. Stored Ca^{2+} depletion-induced oligomerization of stromal interaction molecule 1 (STIM1) via the EF-SAM region: an initiation mechanism for capacitive Ca^{2+} entry. *J Biol Chem*. 2006;281(47):35855-35862.
3. Zhang SL, Yu Y, Roos J, et al. STIM1 is a Ca^{2+} sensor that activates CRAC channels and migrates from the Ca^{2+} store to the plasma membrane. *Nature*. 2005;437(7060):902-905.
4. Feske S, Gwack Y, Prakriya M, et al. A mutation in Orai1 causes immune deficiency by abrogating CRAC channel function. *Nature*. 2006;441(7090):179-185.
5. Wang WA, Demaurex N. Proteins interacting with STIM1 and store-operated Ca^{2+} entry. *Prog Mol Subcell Biol*. 2021;59:51-97.

6. Lee SK, Lee MH, Jeong SJ, et al. The inactivation domain of STIM1 acts through intramolecular binding to the coiled-coil domain in the resting state. *J Cell Sci*. 2020;133(1):jcs237354.

7. Böhm J, Chevessier F, Maues De Paula A, et al. Constitutive activation of the calcium sensor STIM1 causes tubular-aggregate myopathy. *Am J Hum Genet*. 2013;92(2):271-278.

8. Böhm J, Chevessier F, Koch C, et al. Clinical, histological and genetic characterisation of patients with tubular aggregate myopathy caused by mutations in STIM1. *J Med Genet*. 2014;51(12):824-833.

9. Hedberg C, Niceta M, Fattori F, et al. Childhood onset tubular aggregate myopathy associated with de novo STIM1 mutations. *J Neurol*. 2014;261(5):870-876.

10. Nesin V, Wiley G, Kousi M, et al. Activating mutations in STIM1 and ORAI1 cause overlapping syndromes of tubular myopathy and congenital miosis. *Proc Natl Acad Sci USA*. 2014;111(11):4197-4202.

11. Endo Y, Noguchi S, Hara Y, et al. Dominant mutations in ORAI1 cause tubular aggregate myopathy with hypocalcemia via constitutive activation of store-operated Ca^{2+} channels. *Hum Mol Genet*. 2015;24(3):637-648.

12. Michelucci A, García-Castañeda M, Boncompagni S, Dirksen RT. Role of STIM1/ORAI1-mediated store-operated Ca^{2+} entry in skeletal muscle physiology and disease. *Cell Calcium*. 2018;76:101-115.

13. Picard C, McCarl CA, Papolos A, et al. STIM1 mutation associated with a syndrome of immunodeficiency and autoimmunity. *N Engl J Med*. 2009;360(19):1971-1980.

14. Morin G, Biancalana V, Echaniz-Laguna A, et al. Tubular aggregate myopathy and Stormorken syndrome: mutation spectrum and genotype/phenotype correlation. *Hum Mutat*. 2020;41(1):17-37.

15. Okuma H, Saito F, Mitsui J, et al. Tubular aggregate myopathy caused by a novel mutation in the cytoplasmic domain of STIM1. *Neurol Genet*. 2016;2(1):e50.

16. Kim JH, Carreras-Sureda A, Didier M, Henry C, Frieden M, Demaurex N. The TAM-associated STIM1^{I484R} mutation increases ORAI1 channel function due to a reduced STIM1 inactivation break and an absence of microtubule trapping. *Cell Calcium*. 2022;105:102615.

17. Takahashi K, Tanabe K, Ohnuki M, et al. Induction of pluripotent stem cells from adult human fibroblasts by defined factors. *Cell*. 2007;131(5):861-872.

18. Nakagawa M, Koyanagi M, Tanabe K, et al. Generation of induced pluripotent stem cells without Myc from mouse and human fibroblasts. *Nat Biotechnol*. 2008;26(1):101-106.

19. Okita K, Matsumura Y, Sato Y, et al. A more efficient method to generate integration-free human iPS cells. *Nat Methods*. 2011;8(5):409-412. doi:10.1038/nmeth.1591

20. Nalbandian M, Zhao M, Sasaki-Honda M, et al. Characterization of hiPSC-derived muscle progenitors reveals distinctive markers for myogenic cell purification toward cell therapy. *Stem Cell Rep*. 2021;16(4):883-898.

21. Yu J, Hu K, Smuga-Otto K, et al. Human induced pluripotent stem cells free of vector and transgene sequences. *Science*. 2009;324(5928):797-801.

22. Sakai-Takemura F, Narita A, Masuda S, et al. Premyogenic progenitors derived from human pluripotent stem cells expand in floating culture and differentiate into transplantable myogenic progenitors. *Sci Rep*. 2018;8(1):6555.

23. Chal J, Oginuma M, Al Tanoury Z, et al. Differentiation of pluripotent stem cells to muscle fiber to model Duchenne muscular dystrophy. *Nat Biotechnol*. 2015;33(9):962-969.

24. Chal J, Pourquié O. Making muscle: skeletal myogenesis *in vivo* and *in vitro*. *Development*. 2017;144(12):2104-2122.

25. Hosoyama T, McGivern JV, Van Dyke JM, Ebert AD, Suzuki M. Derivation of myogenic progenitors directly from human pluripotent stem cells using a sphere-based culture. *Stem Cells Transl Med*. 2014;3(5):564-574.

26. Sakai-Takemura F, Nogami K, Elhussieny A, et al. Prostaglandin EP2 receptor downstream of Notch signaling inhibits differentiation of human skeletal muscle progenitors in differentiation conditions. *Commun Biol*. 2020;3(1):182.

27. Elhussieny A, Nogami K, Sakai-Takemura F, et al. Mesenchymal stem cells derived from human induced pluripotent stem cells improve the engraftment of myogenic cells by secreting urokinase-type plasminogen activator receptor (uPAR). *Stem Cell Res Ther*. 2021;12(1):532.

28. Darbellay B, Arnaudeau S, Bader CR, Konig S, Bernheim L. STIM1L is a new actin-binding splice variant involved in fast repetitive Ca^{2+} release. *J Cell Biol*. 2011;194(2):335-346.

29. Nogami K, Maruyama Y, Sakai-Takemura F, et al. Pharmacological activation of SERCA ameliorates dystrophic phenotypes in dystrophin-deficient mdx mice. *Hum Mol Genet*. 2021;30(11):1006-1019.

30. Xi H, Langerman J, Sabri S, et al. A human skeletal muscle atlas identifies the trajectories of stem and progenitor cells across development and from human pluripotent stem cells. *Cell Stem Cell*. 2020;27(1):181-185.

31. Uezumi A, Nakatani M, Ikemoto-Uezumi M, et al. Cell-surface protein profiling identifies distinctive markers of progenitor cells in human skeletal muscle. *Stem Cell Rep*. 2016;7(2):263-278.

32. Popp MW, Maquat LE. Leveraging rules of nonsense-mediated mRNA decay for genome engineering and personalized medicine. *Cell*. 2016;165(6):1319-1322.

33. Lindeboom RGH, Vermeulen M, Lehner B, Supek F. The impact of nonsense-mediated mRNA decay on genetic disease, gene editing and cancer immunotherapy. *Nat Genet*. 2019;51(11):1645-1651.

34. Dörr K, Kilch T, Kappel S, et al. Cell type-specific glycosylation of Orai1 modulates store-operated Ca^{2+} entry. *Sci Signal*. 2016;9(418):ra25.

35. Gwack Y, Srikanth S, Feske S, et al. Biochemical and functional characterization of Orai proteins. *J Biol Chem*. 2007;282(22):16232-16243.

36. Suzuki J, Kanemaru K, Ishii K, Ohkura M, Okubo Y, Iino M. Imaging intraorganellar Ca^{2+} at subcellular resolution using CEPIA. *Nat Commun*. 2014;5:4153.

37. Mensch A, Zierz S. Cellular stress in the pathogenesis of muscular disorders-from cause to consequence. *Int J Mol Sci*. 2020;21(16):5830.

38. Snapp EL, Hegde RS, Francolini M, et al. Formation of stacked ER cisternae by low affinity protein interactions. *J Cell Biol*. 2003;163(2):257-269.

39. Kudo T, Kanemoto S, Hara H, et al. A molecular chaperone inducer protects neurons from ER stress. *Cell Death Differ*. 2008;15(2):364-375.

40. Korzeniowski MK, Popovic MA, Szentpetery Z, Varnai P, Stojilkovic SS, Balla T. Dependence of STIM1/Orai1-mediated

calcium entry on plasma membrane phosphoinosities. *J Biol Chem*. 2009;284(31):21027-21035.

41. Maléth J, Choi S, Muallem S, Ahuja M. Translocation between PI(4,5)P2-poor and PI(4,5)P2-rich microdomains during store depletion determines STIM1 conformation and Orai1 gating. *Nat Commun*. 2014;5:5843.

42. Lewis RS. Store-operated calcium channels: from function to structure and back again. *Cold Spring Harb Perspect Biol*. 2020;12(5):a035055.

43. Zhou Y, Srinivasan P, Razavi S, et al. Initial activation of STIM1, the regulator of store-operated calcium entry. *Nat Struct Mol Biol*. 2013;20(8):973-981.

44. Fahrner M, Muik M, Schindl R, et al. A coiled-coil clamp controls both conformation and clustering of stromal interaction molecule 1 (STIM1). *J Biol Chem*. 2014;289(48):33231-33244.

45. Engel WK, Bishop DW, Cunningham GG. Tubular aggregates in type II muscle fibers: ultrastructural and histochemical correlation. *J Ultrastruct Res*. 1970;31(5–6):507-525.

46. Sánchez-González C, Herrero Martín JC, Salegi Ansa B, et al. Chronic inhibition of the mitochondrial ATP synthase in skeletal muscle triggers sarcoplasmic reticulum distress and tubular aggregates. *Cell Death Dis*. 2022;13(6):561.

47. Agbulut O, Destombes J, Thiesson D, Butler-Browne G. Age-related appearance of tubular aggregates in the skeletal muscle of almost all male inbred mice. *Histochem Cell Biol*. 2000;114(6):477-481.

48. Boncompagni S, Protasi F, Franzini-Armstrong C. Sequential stages in the age-dependent gradual formation and accumulation of tubular aggregates in fast twitch muscle fibers: SERCA and calsequestrin involvement. *Age (Dordr)*. 2012;34(1):27-41.

49. Giacomello E, Crea E, Torelli L, et al. Age dependent modification of the metabolic profile of the tibialis anterior muscle fibers in C57BL/6J mice. *Int J Mol Sci*. 2020;21(11):3923.

50. Preissler S, Rato C, Yan Y, Perera LA, Czako A, Ron D. Calcium depletion challenges endoplasmic reticulum proteostasis by destabilising BiP-substrate complexes. *Elife*. 2020;9:e62601.

51. Lièvremont JP, Rizzuto R, Hendershot L, Meldolesi J. BiP, a major chaperone protein of the endoplasmic reticulum lumen, plays a direct and important role in the storage of the rapidly exchanging pool of Ca^{2+}. *J Biol Chem*. 1997;272(49):30873-30879.

52. Schäuble N, Lang S, Jung M, et al. BiP-mediated closing of the Sec61 channel limits Ca^{2+} leakage from the ER [published correction appears in *EMBO J*. 2012;31(18):3784]. *EMBO J*. 2012;31(15):3282-3296.

53. Daverkausen-Fischer L, Pröls F. Regulation of calcium homeostasis and flux between the endoplasmic reticulum and the cytosol. *J Biol Chem*. 2022;298(7):102061.

SUPPORTING INFORMATION

Additional supporting information can be found online in the Supporting Information section at the end of this article.